Performance of the GSN station ALE-II, 1990-2009

A report in a series documenting the status of the Global Seismographic Network

WQC Report 2010:3
January 15, 2010

Göran Ekström and Meredith Nettles

Waveform Quality Center
Lamont-Doherty Earth Observatory of Columbia University, New York

1 Station performance report: ALE

This report summarizes a number of observations that are relevant for assessing the past and current quality of the data recorded at one of the stations of the Global Seismographic Network. The purpose of the report is, in part, to document specific problems observed with the data. Some of these problems are related to errors in the available descriptions of station parameters: orientation of the sensors, response functions, polarities. In principle, such errors in the station metadata can be corrected by providing updated station parameters. In practice, this may be difficult in some cases due to lack of knowledge of, or inability to determine, the correct parameters. Other problems are caused by the malfunctioning of some instrument component. Regardless of the cause, it is necessary to document and publicize the lack of accurate and reliable station characteristics, especially when it is not obvious from simple inspection of the data that a problem exists. It is also of value to document the characteristics of stations performing well, both to establish their high quality and to help identify installation and operation procedures that should be emulated at other stations.

1.1 Station ALE

The station ALE (Alert) is located near the northeastern tip of Ellesmere Island, Qikiqtaaluk Region, Canada (see Figure 1). It is the northernmost station in the Global Seismographic Network, and is in an excellent location for providing global coverage in earthquake and Earth structure studies. It is also one of the few GSN stations located close to the source regions of Greenland's glacial earthquakes (Nettles and Ekström, 2010). The closest GSN station is KBS-IU (Kings Bay) on Spitsbergen, approximately 1200 km east of ALE.

ALE is part of the IDA (II) component of the IRIS/USGS Global Seismographic Network and is operated by the IDA group at the University of California, San Diego.

1.2 The data

Digital seismic data from ALE are available from the IRIS DMC beginning in 1990. Here, we consider broadband instruments at the station. The initial installation consisted of a set of STS-1 seismometers. An auxiliary STS-2 sensor was installed in 2003. Data from ALE are included in our standard CMT analysis (Dziewonski et al., 1981; Ekström et al., 2005), and waveform data, travel-time observations, and dispersion curves derived from ALE data have been used in the development of numerous global and regional tomographic models since the station was installed.

In the analyses described here, we have made use of data collected from the IRIS DMC. We requested and downloaded all long-period (LH) and very-long-period (VH) data available at the DMC for both sensors from the start of operation (1990) until August 2009. We used the currently available station metadata prepared by the IDA group in San Diego (downloaded in December 2009) and also available at the IRIS DMC. Overall, the station has been operated with few data outages since 1990.

1.3 The metadata

The dataless SEED volume for ALE documents 4 response epochs for the STS-1 (primary) and STS-2 (secondary) sensors at ALE. The STS-1 1 sps LH channels have location code 00 and we refer to these channels as LHZ-00, LHN-00, and LHE-00. The STS-2 sensor (location code 10) was installed on 2003.228 (228 representing the julian day) and we refer to the 1 sps channels as LHZ-10, LHN-10, and LHE-10. Epoch boundaries are given at 1990.050 (first data), 1993.026, 1995.163, and 2003.228 (first STS-2 data). The metadata indicate gain changes at all epoch boundaries; otherwise, no variations in the frequency response is indicated.

1.4 Scaling analysis

One method for assessing the quality of the data is the systematic comparison of recorded long-period waveforms with synthetic seismograms calculated for known seismic events. This analysis follows the steps described by Ekström et al. (2006). Seismic data for the LH and VH channels from both the STS-1 and STS-2 sensors are collected. Corresponding synthetic waveforms for all earthquakes in the Global CMT catalog (Dziewonski et al., 1981; Ekström et al., 2005) with $M_W \geq 6.5$ are calculated. Correlation coefficients and optimal scaling factors between observed and synthetic waveforms are calculated for the three types of data used in the standard CMT analysis: body waves (B), with periods in the range 50–150 sec, mantle waves (M), with periods in the range 125–350 sec, and surface waves (S), with periods in the range 50–150 sec. The scaling factor is only calculated for waveforms with a correlation of 0.75 or greater. The scaling factor is the number by which the synthetic seismogram should be multiplied to maximize the agreement with the observed seismogram. Annual median values of the scaling factors are calculated when four or more individual event scaling estimates are available for the year. Reversed components can be identified by their large negative correlations.

Figure 2 shows the results of our systematic comparison of ALE waveforms with synthetic seismograms. From the start of operation in 1990 until late 1992 or early 1993, the observed STS-1 seismograms correlate well with the synthetic waveforms, but the amplitudes are too large by a large factor (larger than 2.0). This problem disappears in 1993, and the seismogram scaling factors for the period 1993–present are consistent and stable for all STS-1 channels. The STS-2 seismometer, installed in 2003, also generates seismograms that scale well with respect to the synthetic waveforms.

1.5 Noise analysis

A second method for investigating the overall performance of the sensors is to monitor background noise levels for all seismic channels, after conversion of the data to ground acceleration. We calculate hourly rms values of the time-domain seismic signal in narrow frequency bands, and convert the rms values to a power spectral density (PSD) at that frequency using Parseval's theorem. For each month, we then calculate the low-noise value at each frequency by determining the PSD amplitude not exceeded 10% of the time.

The PSD data provide much information about the station and the sensors. Figure 3 shows the monthly low-noise estimate for each LH channel at 72-s period since 1990. The first observation is that the station has been providing data without major outages since 1990. Only in 1992 and 1993 are there gaps of a few months. Second, the noise data suggest that ALE generally is a very quiet site, and that the noise characteristics have remained stable since 1994. Third, there is a clear problem with the STS-1 data prior to 1993. The high noise values of all three components suggest that the gains are overstated in the metadata by a factor of $\sim$5–10.

The STS-2 noise levels are similar to those of the STS-1 at 72-s period. There is a suggestion in the data that horizontal noise levels on the STS-1 increased at the time of installation of the STS-2 sensor, and that vertical noise levels decreased (at least the lowest annual values). The vertical STS-2 channel (LHZ-10) has become noisier since installation.

1.6 Inter-sensor coherence

An additional method for assessing the quality and calibration of the recorded signals is to calculate inter-sensor coherence. This analysis is possible when more than one sensor is operated in the same location. At ALE, this is possible for the period 2003–2009, during which time both STS-1 and STS-2 instruments have been operating.

We calculate the coherence of the deconvolved vertical, N–S, and E–W components. The coherence is calculated for $\sim$2-hour-long time windows containing the signals for earthquakes with $M_W \geq 6.5$ (the same events used in the scaling analysis). For each pair of seismograms, the coherence is calculated in narrow frequency bands around 32 s, 64 s, 128 s and 256 s. If the coherence is greater than 0.95, the value is stored together with the complex scaling factor (represented here as a scaling factor and phase shift) that should be applied to the secondary-sensor data to bring the two time series into the best agreement. In the following, the discussion is based on the assumption that the secondary (STS-2) sensor is properly calibrated and that deviations from a scaling factor of 1.0 and a phase shift of 0° should be attributed to differences between the true and reported response functions of the primary (STS-1) sensor.

Figure 4 shows the results of the coherence analysis for the vertical component. The measurements are very consistent and stable, with a scaling factor close to 1.0 for all periods, and a phase shift close to 0°. Nearly all scaling values are slightly smaller than 1.0, suggesting that the true gain of the STS-1 may be 1–3% less than stated in the metadata.

The horizontal components show results that are similar to those of the vertical. Figure 5 shows the amplitude and phase differences for the N–S components. A scatter of scaling measurements corresponding to gain variations of a few percent is seen with a possible annual periodicity. These variations are, however, very small. In addition, there is a slight suggestion that deviations towards smaller values are more common at the longer periods (128 s and 256 s). We are hesitant to attribute significance to these small deviations.

Figure 6 shows the results for the E–W component, which are similar to those of the N–S component. In general, the measurements are consistent with stable instrument responses during the time period. In detail, we note that the scatter of scaling values is slightly larger than for the N–S component, and noticeably larger

than for the vertical component. Given that we use the same selection criteria for the coherence for the three components, we do not yet understand this difference in scatter.

1.7 Polarization analysis

The orientation of the horizontal components can be assessed empirically by comparing observed and synthetic waveforms, and finding the angle by which the horizontal components should be rotated in order to maximize the agreement. We follow the approach described by Ekström and Busby (2008) for such a comparison, using the observed and synthetic waveforms from Global CMT analysis.

We apply the method of Ekström and Busby (2008) to the same dataset used in the scaling analysis. Figure 7 shows the individual measurements for the period of operation for the different channels. Overall, the number of useful observations is large, a consequence of the low level of horizontal noise at ALE. No polarization observations are obtained for 1990–1992, since the instrument gains for this period are incorrect. The median rotation angles for the STS-1 and the STS-2 sensors are both 0°, and the spreads of observations are small. The median estimates for the entire period of operation are given in Table 1.

Comp. 1	Comp. 2	First	Last	# Obs.	N	Az 1	Az 2	25%	Med.	75%
LHE-00	LHN-00	19900303	20090623	664	171	90	0	-4	0	5
LHE-10	LHN-10	20030921	20090623	246	74	90	0	-4	0	3

Table 1: Statistics of sensor-rotation angles estimated in this study. Columns are the channel names, the dates of the first and last observations considered in making the estimate, the total number of observations, the number of observations of acceptable quality, the reported azimuths of sensitivity of the two channels, the median polarization-angle deviation from the reported orientation together with the range of the second (25%) and third (75%) quartiles of the observations.

1.8 Example seismograms

The anomalies described here agree with observations we have made in our routine analysis of waveforms for the determination of CMT earthquake parameters. When confronted with the seismograms for an individual earthquake, it is often difficult to assess whether a poor fit is due to incorrect source parameters, inadequate modeling of wave propagation through an Earth model, or some problem with the recorded seismograms. Here, we have included some examples of data that illustrate the characteristics of the types of problems that we have encountered with data from the ALE station.

Figure 8 shows an example of three-component mantle-wave data for an earthquake on June 9, 1991. This corresponds to the period during which we find that there is a gain problem with the data (Figure 2 and Figure 3). The correlation between the observed and synthetic waveforms is high, but there is a difference in amplitude of $\sim$8. Apart from the gain, the observed waveforms agree well with the synthetic waveforms.

The top panel of Figure 9 shows a comparison between surface-wave seismograms recorded on the STS-1 seismometer and the corresponding synthetic waveforms for an event on June 23, 2009. The waveforms are nicely matched. The bottom panel of Figure 9 shows the comparison between seismograms recorded on the STS-2 seismometer and the corresponding synthetic waveforms for the same event. The fits are also good for all components for this sensor. The main difference between the STS-1 and STS-2 seismograms is the presence of some noise pulses on the STS-2 records.

2 Summary and analysis

At the time of writing (January, 2010), the GSN station ALE is performing very well. Our analysis suggests that the station has been producing GSN quality data consistently since 1993, and that the STS-2 provides high-quality backup data streams.

Our scaling analysis (Figure 2) and noise analysis (Figure 3) indicate that the frequency-independent gain is incorrectly specified in the station metadata for the period 1990–1992. The coherence analysis for the vertical component may indicate a relative gain difference of 1-3% between the STS-1 and STS-2. Low-amplitude variations are seen in the coherence analysis of the horizontal components, but these are very small. We do not understand the larger scatter (still small) of coherence measurements for the E–W component compared with those of the N–S and vertical components.

3 Conclusions and recommendations

This analysis shows that ALE currently is generating data of high quality. While more detailed analysis would be required to establish that the response characteristics are accurate to within the 1% tolerance of the original GSN design goals (IRIS, 1985; Lay et al., 2002), our assessment is that, at least at long periods, ALE generates GSN quality data and has done so consistently since 1993.

The STS-1 gain specified prior to 1993 should be reassessed. It might be useful to try to identify the noise pulses on the STS-2 horizontal components (Figure 9).

We note that there is no indication that the STS-1 at ALE is suffering from the long-period gain loss documented at several other stations equipped with STS-1 seismometers (Ekström et al., 2006). To the extent that it is possible to identify installation details or operational procedures that could have contributed to the elimination (or delayed onset) of this problem, it would be useful to document these and modify other installations accordingly.

4 References

Dziewonski, A. M., T.-A. Chou, and J. H. Woodhouse, Determination of earthquake source parameters from waveform data for studies of global and regional seismicity, *J. Geophys. Res.*, 86, 2825–2853, 1981.

Ekström, G., A. M. Dziewonski, N. N. Maternovskaya, and M. Nettles, Global seismicity of 2003: Centroid-moment tensor solutions for 1087 earthquakes, *Phys. Earth Planet. Inter.*, 148, 327–351, 2005.

Ekström, G., C. A. Dalton, and M. Nettles, Observations of time-dependent errors in long-period gain at global seismic stations, *Seism. Res. Lett.*, 77, 12–22, 2006.

Ekström, G., and R. W. Busby, Measurements of seismometer orientation at USArray Transportable and Backbone stations, *Seism. Res. Lett.*, 79, 554-561, 2008.

IRIS, *The design goals for a new global seismographic network*, IRIS GSN committee report, 31 pages, 1985.

Lay, T., J. Berger, R. Buland, R. Butler, G. Ekström, B. Hutt, B. Romanowicz, *Global seismic network design goals update 2002*, IRIS GSN committee report, 2002.

Nettles, M., and G. Ekström, Glacial earthquakes in Greenland and Antarctica, *Annual Reviews*, in review, 2010.

Peterson, J., Observations and modeling of background seismic noise, *U. S. Geol. Surv. Open-file Rep. 93-322*, 1–45, 1993.

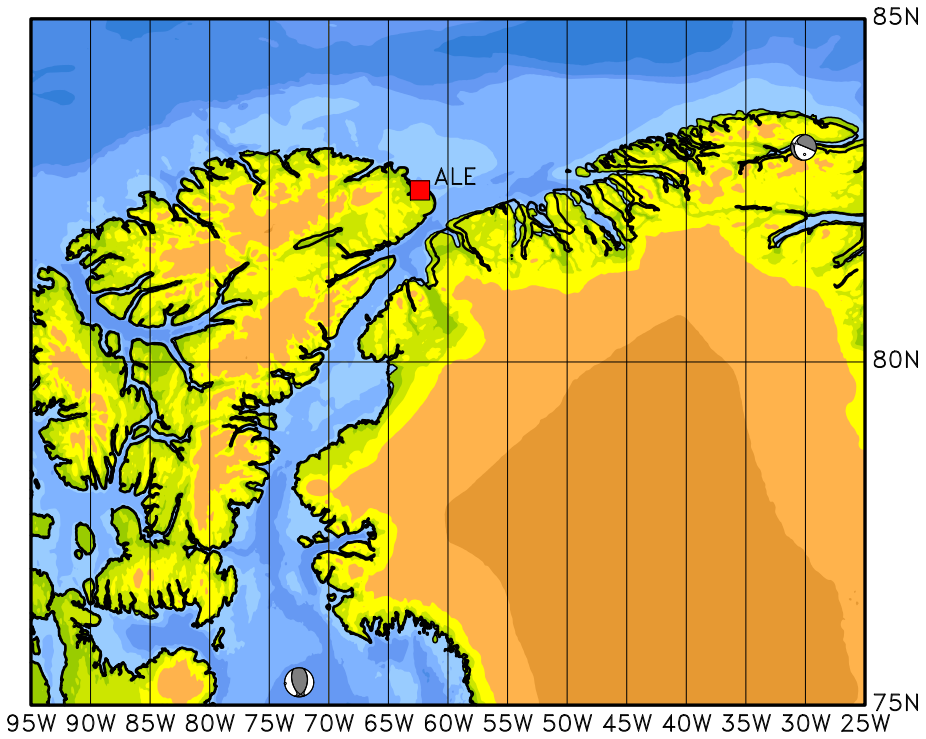

Figure 1: Map showing the location of ALE (red square) in the Qikiqtaaluk Region of northern Canada. Grey focal mechanisms show the locations and moment tensors of earthquakes in the Global CMT catalog. The closest GSN station is KBS-IU, located ∼1200 km to the east on the island of Spitsbergen.

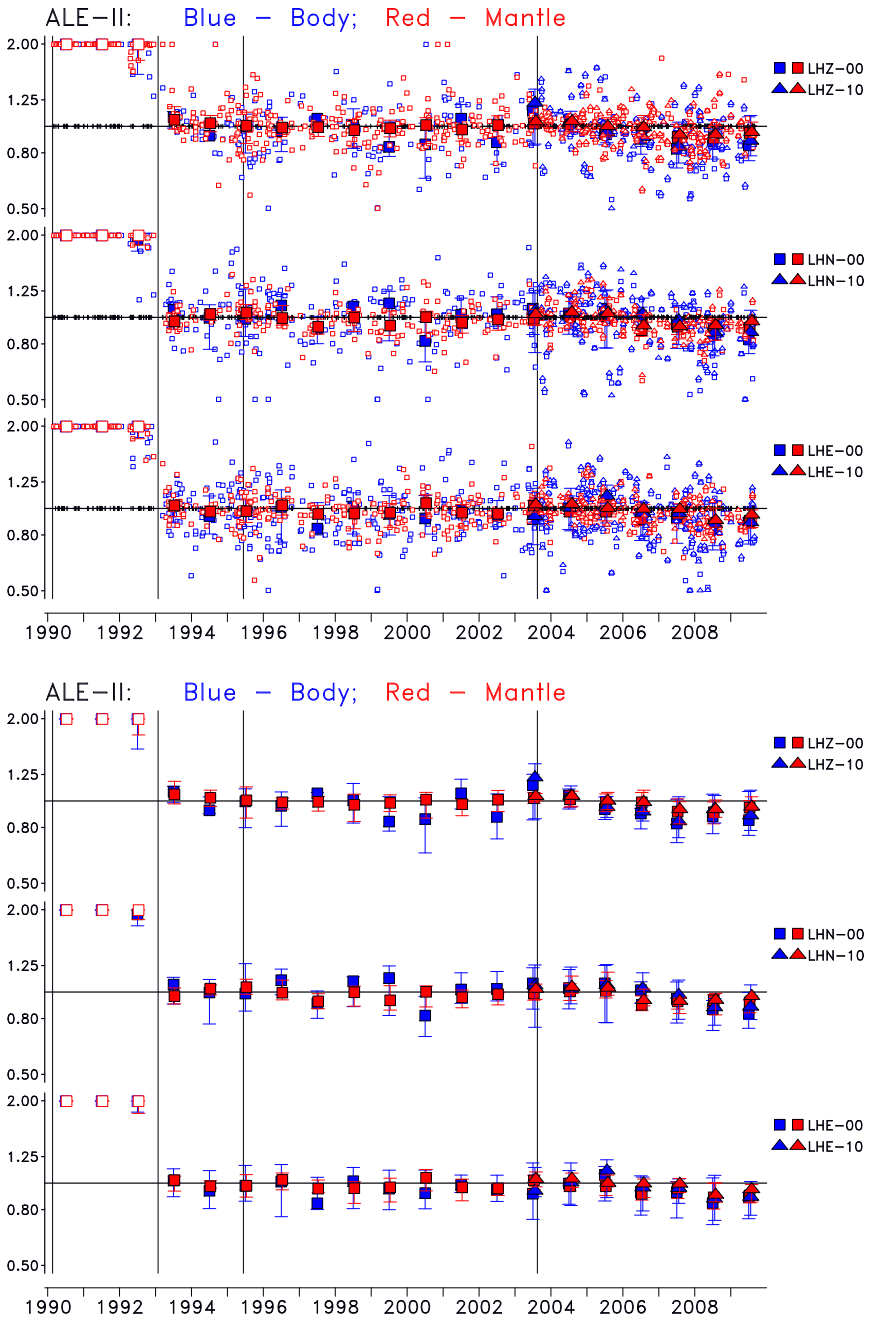

Figure 2: Scaling factors for the various data channels at ALE. Small symbols in top panel show scaling factors for individual traces. Tick marks on the horizontal axes show times of observations for which the correlation was less than 0.75. Large symbols show the median scaling factor for each year, with the error bars corresponding to the range of the second and third quartiles of the scaling factors. The legend on the right identifies the symbol type with a specific channel. Open large symbols indicate that the annual scaling factor was greater than 2.0 (e.g., in 1990–1992). Thin vertical lines show the response epoch boundaries present in the metadata. Bottom panel: same, but showing only the annual median values.

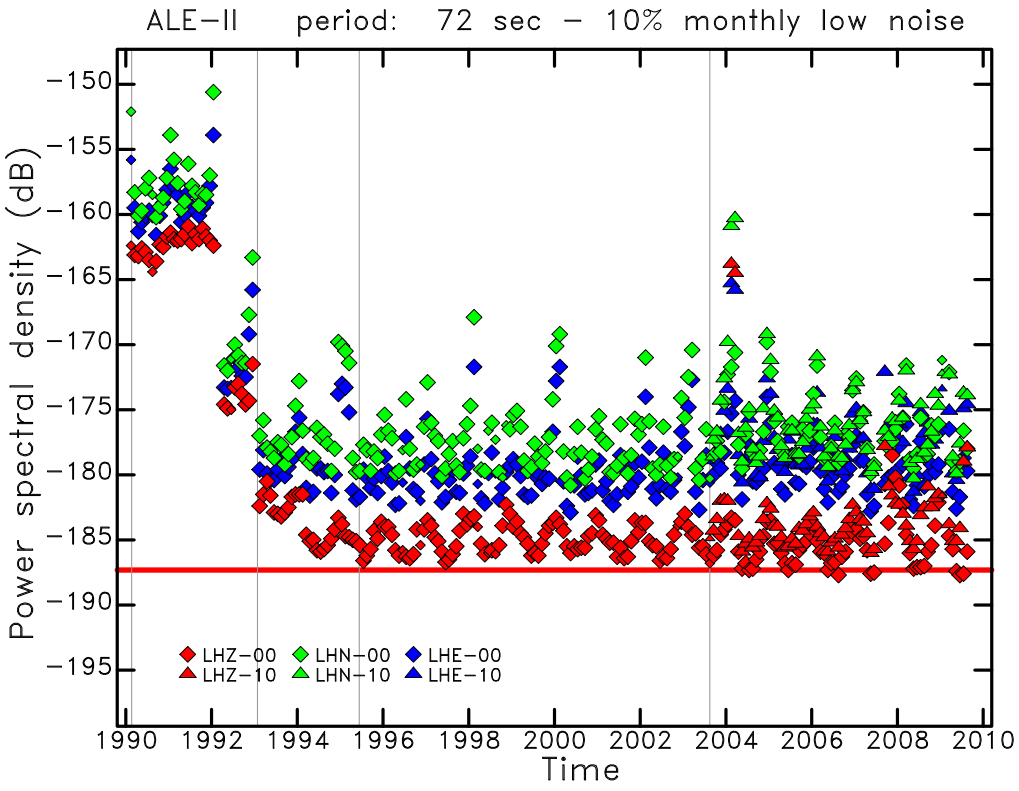

Figure 3: Monthly PSD of ground acceleration at 72-s period for all long-period (LH) channels at ALE for the period 1990–2009. Smaller symbols are used for months with fewer available hourly measurements. Each component and sensor is represented by a distinct symbol and color. The red horizontal line indicates the level of Peterson's (1993) Low Noise Model (LNM) at 72 s. The thin vertical lines show the times of epoch boundaries in the station metadata.

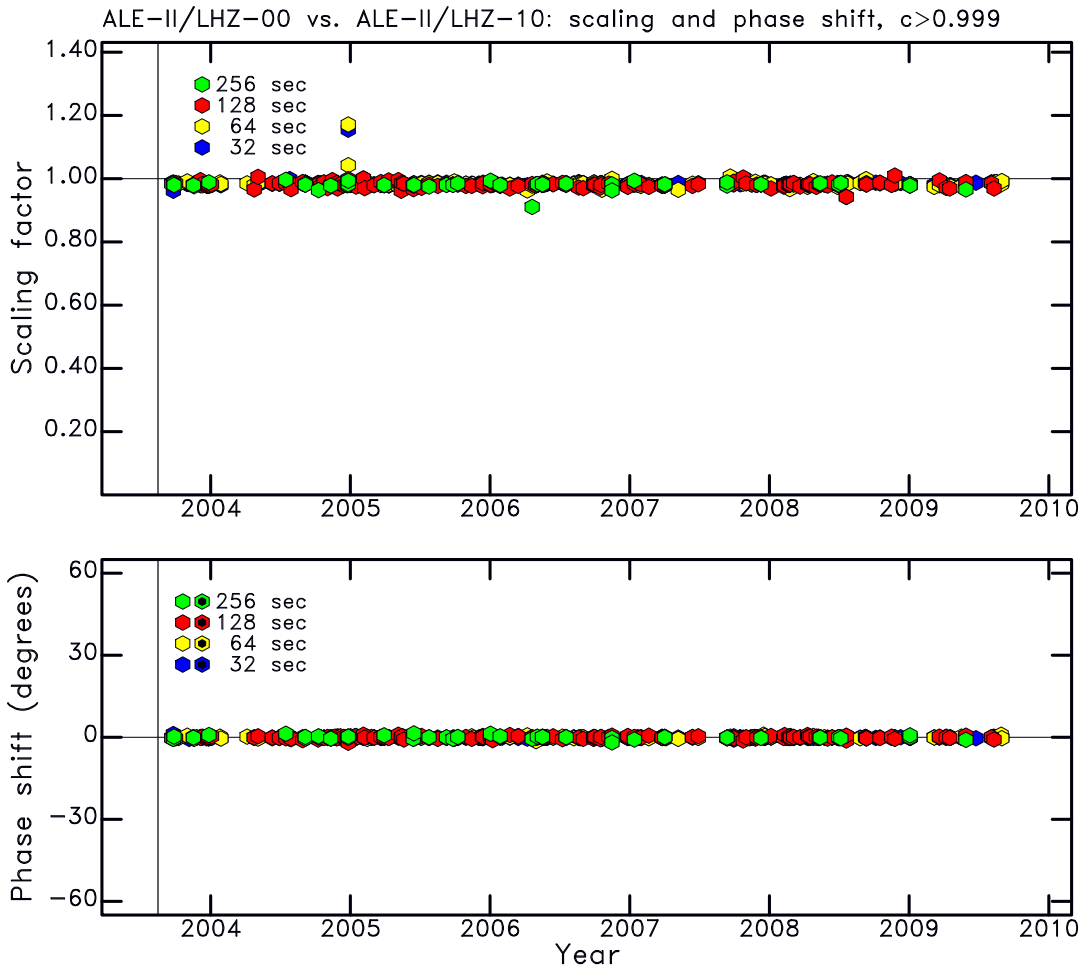

Figure 4: Diagram shows the result of coherence analysis for the vertical components of the STS-1 and STS-2 sensors. Each symbol represents a measurement of coherence for a $M_W \geq 6.5$ earthquake. The minimum coherence plotted is indicated by c. The scaling and phase shift between the two time series is shown at four different periods. The small deviations of the coherence measurements from a scaling of 1.0 and a phase shift of 0° show that the calibrations are consistent. The thin vertical lines show the times of epoch boundaries in the station metadata.

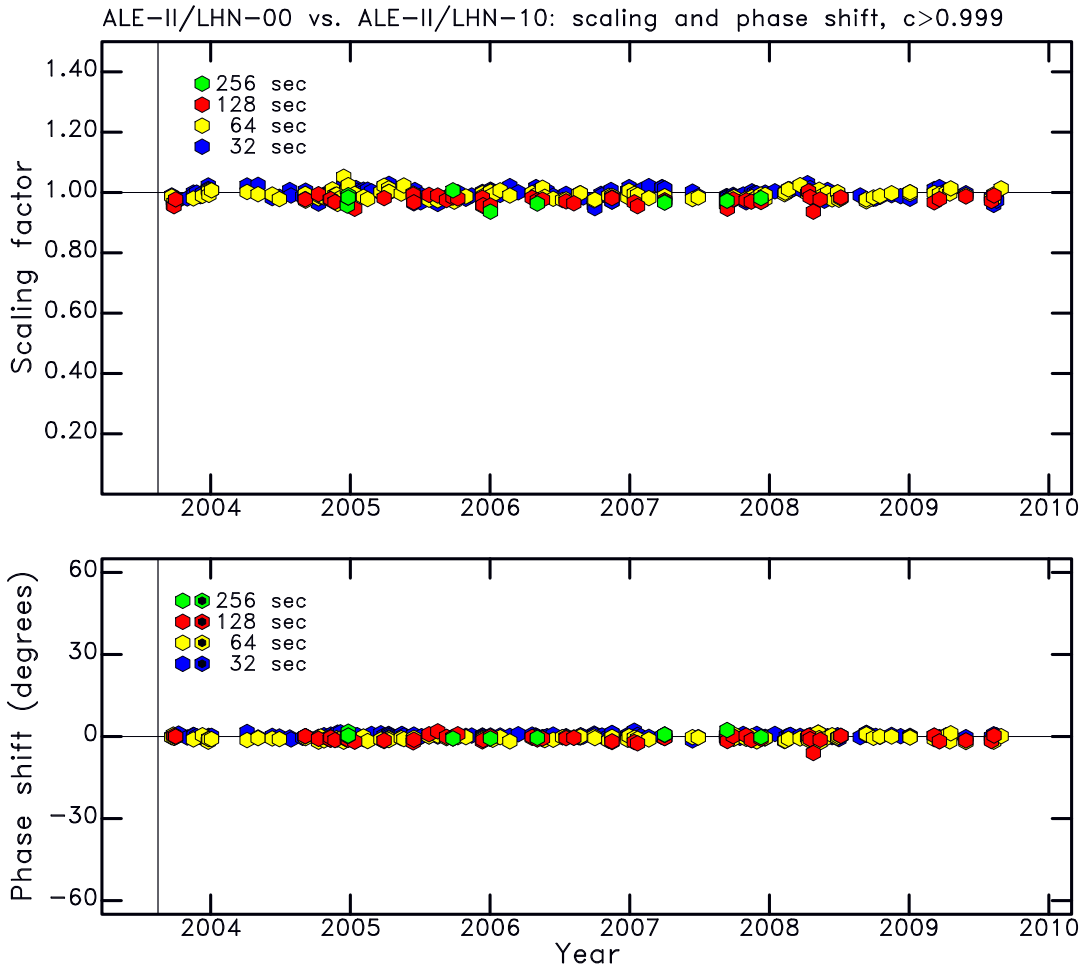

Figure 5: Same as Figure 4, but for the North-South components. Small, possibly seasonal, oscillations are seen in the coherence measurements.

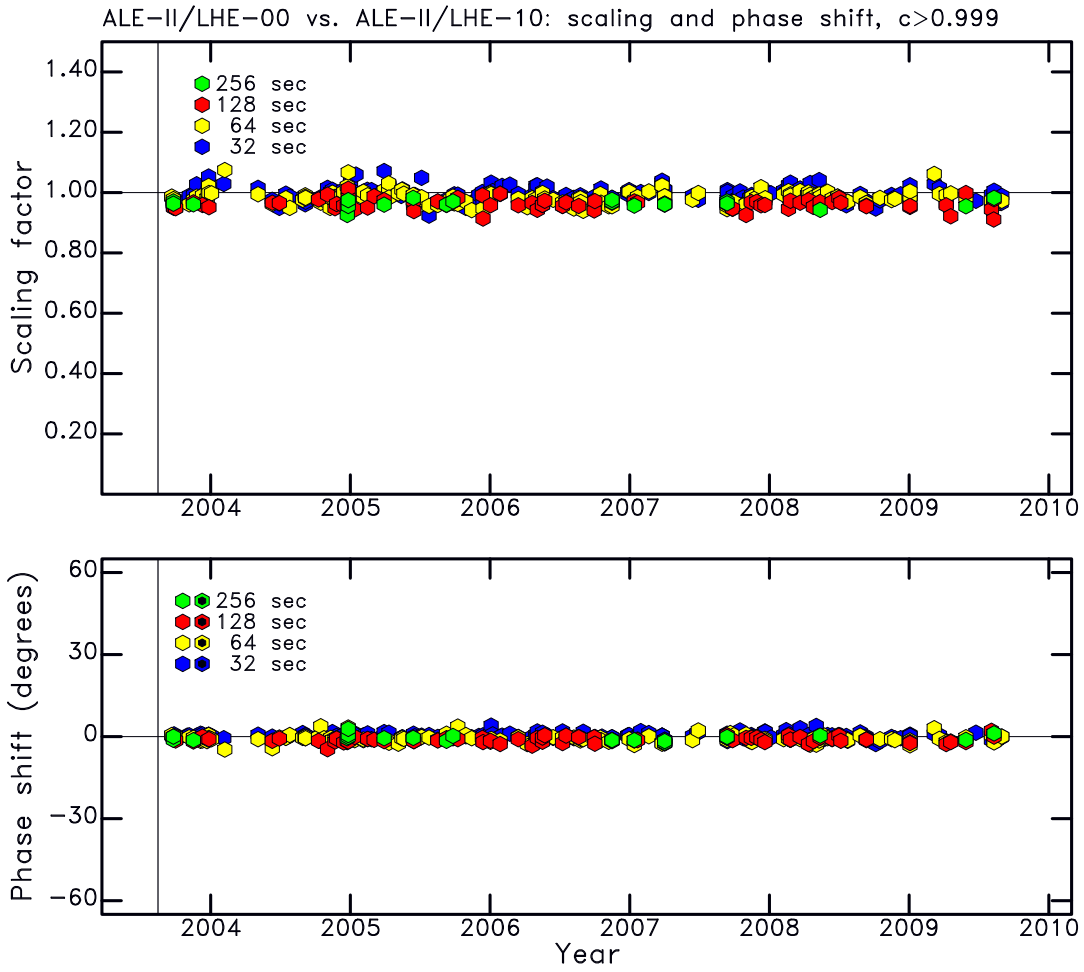

Figure 6: Same as Figure 4, but for the East-West components.

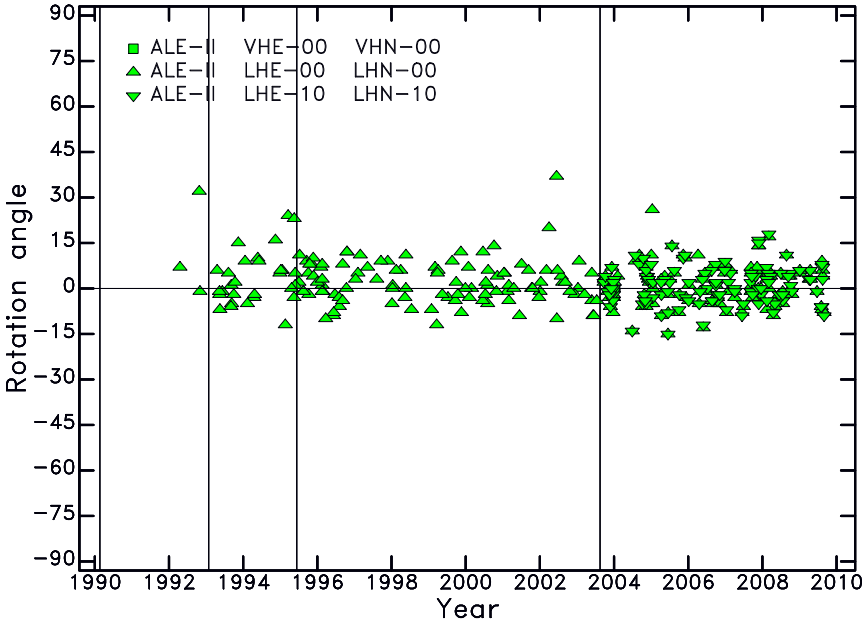

Figure 7: Individual measurements of polarization angle as a function of time. All measurements for the period of operation are shown. No measurements were possible in 1990–1992 since the gain information in the metadata is incorrect for this time period. Symbols represent measurements obtained in the surface-wave band of the CMT analysis. More than 50% of the observations lie in the range -4° to $+5^\circ$. The thin vertical lines show the times of epoch boundaries in the station metadata.

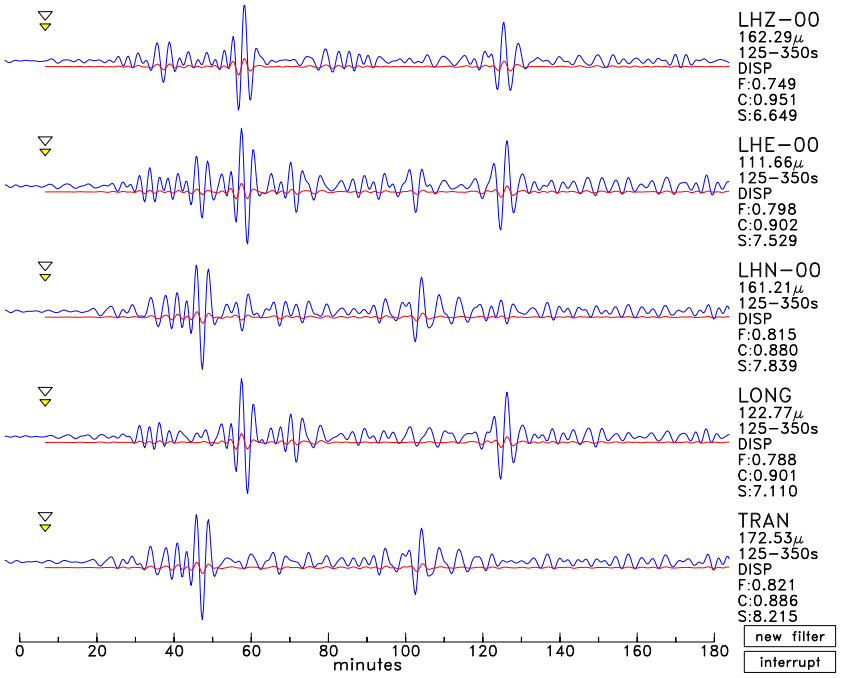

Figure 8: Comparison of observed (blue traces) and synthetic (red traces) mantle-wave seismograms for an earthquake on June 9, 1991. The channel name, maximum displacement, and values for the three parameters residual misfit (F), correlation (C) and scaling factor (S) are given to the right of each waveform. All channels have amplitudes that are different from those of the synthetics by a factor of $\sim$8. The correlation is high, indicating that it is likely that the problem is caused by a frequency-independent gain-factor error.

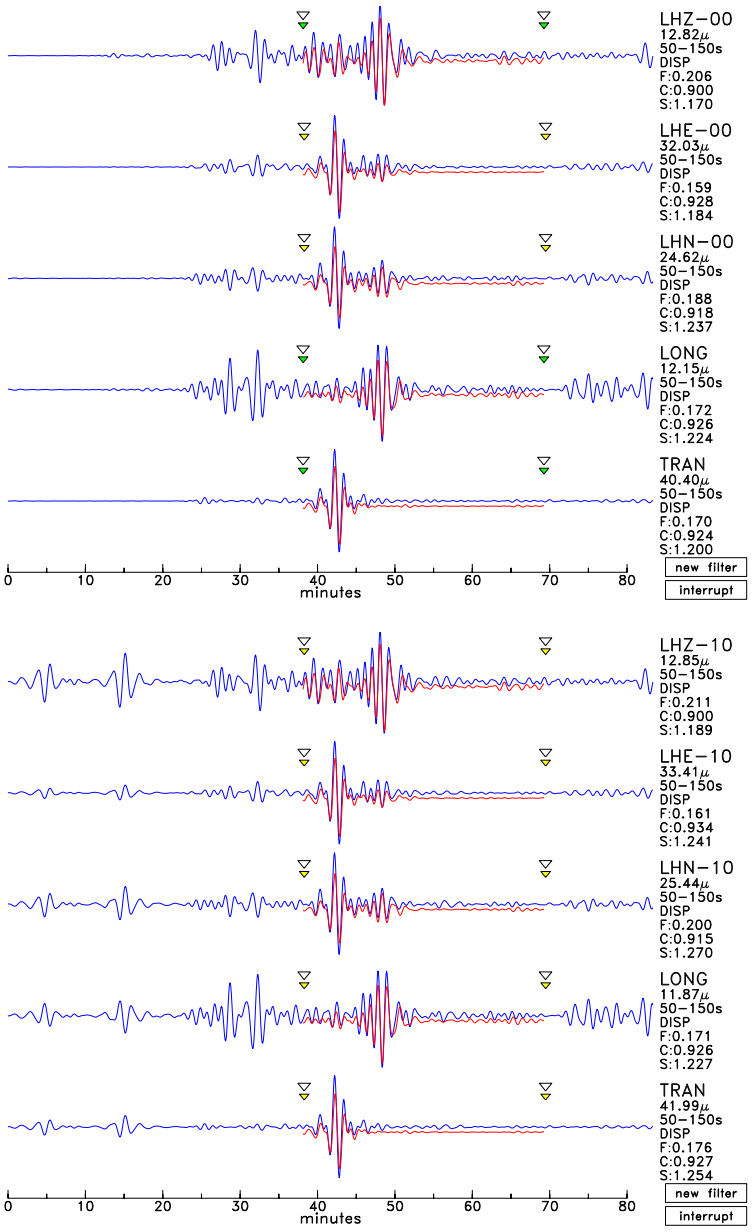

Figure 9: (Top) Observed (STS-1) and synthetic surface-wave seismograms for an earthquake on June 23, 2009. The fit is very good. (Bottom) Observed (STS-2) and synthetic body-wave seismograms for the same earthquake, but recorded on the STS-2 seismometer. The fit to all three components is good, and the scaling factors for each component are very similar to those of the corresponding STS-1 seismograms. Some noise pulses are seen in the STS-2 data that are not present in the STS-1 seismograms.